Arctic Science

OPEN ACCESS | Research Article

Modelling air, ground surface, and permafrost temperature variability across four dissimilar valleys, Yukon, Canada

Madeleine C. Garibaldi[a], **Philip P. Bonnaventure**[a], **Nick C. Noad**[a], **and Will Kochtitzky**[b]

[a]Department of Geography and Environment, University of Lethbridge, Lethbridge, AB T1K 3M4, Canada; [b]School of Marine and Environmental Programs, University of New England, Biddeford, ME 04005, United States

Corresponding author: **Madeleine C. Garibaldi** (email: madeleine.garibaldi@uleth.ca)

Abstract

Spatial maps of the air and ground thermal regime were generated for four Yukon valleys. The aim was to model air, ground surface, and ground temperature (at fine spatial resolution) using locally measured inverted surface lapse rates (SLR) to better predict temperature along an elevation gradient. These local models were then compared to a regional permafrost probability model, which utilized differing inversion assumptions, as well as circumpolar and national models generated without considering inversions. Overall, permafrost probability in the regional model matched well with the local models where assumptions of treeline and inverted SLRs held true. When normal SLRs were assumed, permafrost presence was overestimated in each valley. This discrepancy was greatest at high elevations where permafrost was predicted to be the coldest and most widespread. However, the difference between valleys was dependent on surface and subsurface characteristics such as higher snow cover, mature forest, or thick organic layers which show a greater disassociation from the air temperature overall. Appropriate characterization of the SLR is essential for accurate predictions of the ground thermal regime's spatial distribution and permafrost presence. These models also provide a starting point for better predictions of warming in these valleys and other areas subject to inversions of similar magnitudes.

Key words: TTOP model, permafrost, Yukon, surface lapse rate, Dempster Highway

1. Introduction

Mountain or alpine permafrost is classified as perennially frozen ground located in mountainous environments but absent from adjacent valleys and lowlands following the reduction in air temperature with elevation (French 2008; Gruber and Haeberli 2009). Permafrost in mountains is especially spatially heterogeneous due to the extreme variability in surface and near surface characteristics (Gruber and Haeberli 2009). This is due to the wide variety of mountain range climatic characteristics with the dominant influence on mountain permafrost possibly differing depending on the mountain range. Elevation, incoming solar radiation, aspect, snow cover, substrate, and cold air circulation have all been cited as the dominant influence on mountain permafrost presence or temperature in different studies (Bonnaventure and Lewkowicz 2008; Gądek and Kędzia 2008; Luetschg et al. 2008; Gruber and Haeberli 2009; Apaloo et al. 2012). Thus, this generalized classification of mountain permafrost may oversimplify the distribution of permafrost in complex topography. This is especially true where the spatial distribution of permafrost is influenced by the presence of temperature inversions. For example, it assumes that increased elevation controls air temperature and does not account for permafrost, whose spatial distribution is highly influenced by the presence of temperature inversions (e.g., Bonnaventure et al. 2012). This increases the complexity of mapping permafrost spatially in these locations. In high-latitude, continental mountains, such as those in Yukon, the presence of persistent winter temperature inversions results in nonlinear permafrost distribution (in relation to elevation). High probabilities of permafrost are present at both low and high elevations, while permafrost is generally absent around treeline (Bonnaventure et al. 2012). This permafrost distribution pattern has been modelled most extensively using the Basal Temperature of Snow (BTS) method, allowing for the creation of permafrost probability surfaces over large portions of Yukon (Lewkowicz and Ednie 2004; Bonnaventure and Lewkowicz 2008, 2011; Bonnaventure et al. 2012).

Although the relation between air temperature inversions and permafrost probability has been well studied, little is known about the impact of surface air temperature inversions on the spatial distribution of ground surface and permafrost temperatures in these environments. The change in near surface (<1.5 m) air temperature with elevation is known as the surface lapse rate (SLR). Under normal SLR conditions, air temperature decreases with increasing elevation, while

Fig. 1. Map showing the locations of the four study area valleys. Permafrost layer from Brown et al. (2002). Base layer from DigitalGlobe Inc. (Imagery © [2017]). Contains information licenced under the Open Government Licence—Canada. Contains information licensed under the Open Government Licence—Yukon.

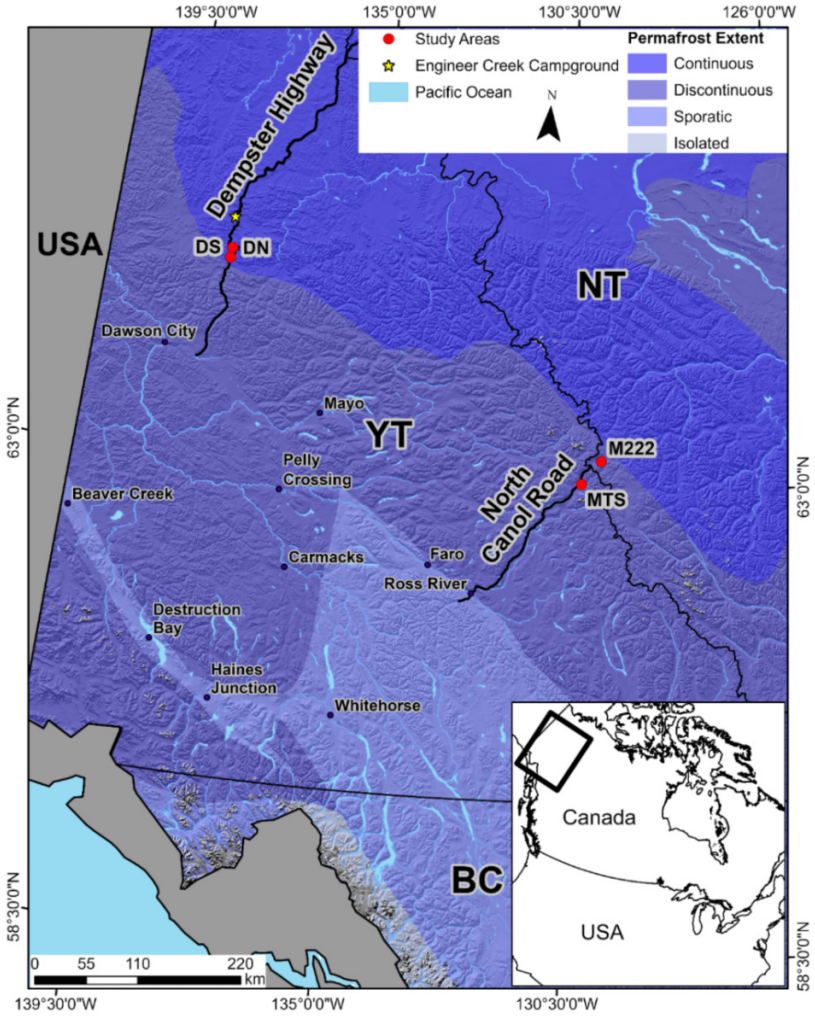

under inverted conditions air temperature increases with increasing elevation. While these permafrost probability studies focused on the southern portion of Yukon where moderate inversions have been observed, recent studies have shown that the magnitude of inversions increases substantially farther north (Noad and Bonnaventure 2022). Additionally, previous studies assumed a lack of surface air temperature inversions in treeless valleys, as SLRs in treed valleys typically become normal above treeline, potentially due to the decrease in surface roughness allowing for wind to disrupt the inversion stability (Wahl 1987; Bonnaventure et al. 2012; Noad and Bonnaventure 2022). However, recent data have shown the presence of these strongly inverted SLRs in valleys even in the absence of trees (Noad and Bonnaventure 2022). Models in this area also substantially underestimated the strength of the inverted SLRs. Lastly, most of the previous work mapping permafrost probability in Yukon was conducted on a regional scale, and did not account for site-specific factors, which may dampen or enhance the impact of air temperature on ground surface and permafrost temperatures.

The first objective of this study was to spatially model air, ground surface, and ground depth temperatures at a fine resolution in four dissimilar valleys in Yukon. This was done to assess the impact of the persistent winter inversions on the ground thermal regime and evaluate how surface cover may modify this impact. A second objective was to assess the performance of a regional model of permafrost probability with differing assumptions of treeline and inversion strength. The results of this study should guide not only current assessment of the ground thermal regime as it relates to elevation, but also present a starting point whereby the pattern of warming with elevation can be evaluated in mountain valleys subject to strong, persistent inversions.

2. Study area

Four unique valleys in Yukon were sampled, two along the Dempster Highway and two along the North Canol Road (Fig. 1). All four valleys are in mountainous terrain with a distinctive elevation range, latitude, vegetation cover, aspect, and valley geometry. The study areas along the Dempster Highway in the Ogilvie Mountains were called Valley Dempster South (Valley DS) and Valley Dempster North (Valley DN),

Table 1. Summary of defining characteristics of each valley.

	Valley floor AMAT (2016/18/19–2021)	Lower SLR	Upper SLR	Relief (m)	Geometry and orientation	Vegetation	Permafrost condition
Valley DS	−6.2	8.3 11.6		700	Two slopes south-facing north-facing	Forested on one slope and unforested on the other	Continuous
Valley DN	−4.4	4.7 1.7		520	Two slopes east facing west facing	Treeless	Continuous
Valley M222	−6.5	10.8	−1.4	570	One slope north facing	Shrubs at lower elevations transitioning to moss and lichen	Extensive discontinuous
Valley MTS	−5.9	10.4	−4.8	805	One slope south-east facing	Mature black spruce forest transitioning to alpine tundra	Extensive discontinuous

Note: Annual mean air temperature (AMAT) is the temperature measured at the lowest station from either 2016, 2018, or 2019 to 2021. The surface lapse rates (SLR) are from the same period as the AMAT for the lower portion of the valley and if recorded the upper portion. Geometry refers to the sampling layout, whether both or only one slope of the valley sampled, and orientation refers to direction the slope(s) is (are) facing. Permafrost condition is from Heginbottom (1995). Valley DS, Valley Dempster South; Valley DN, Valley Dempster North; Valley M222, Valley Mile 222; Valley MTS, Valley MacMillan Transect South.

while the sites along the North Canol in the Selwyn Mountains were named Valley Mile 222 (Valley M222) and Valley MacMillan Transect South (Valley MTS). These valleys were primarily selected based on their distinct characteristics, allowing for an overall comparison of the range of inversions, ground surface temperatures, and permafrost temperatures within the Ogilvie and Mackenzie Mountains in the Yukon. Logistically, these sites were selected based on their accessibility from the road and the existing temperature stations in each location.

The Ogilvie Mountains were last glaciated during the Pre Reid-Glaciation (0.25 myr B.P.) and have remained unglaciated during more recent glacial periods (Yukon Ecoregions Working Group 2004). They are composed of narrow valleys with surface deposits of colluvium and low to moderate segregated and wedge ice (Yukon Ecoregions Working Group 2004; Burn et al. 2015; O'Neill et al. 2019*a*). The climate is sub-arctic continental, and the mountains have moderate relief (typically local relief <800 m) with elevations ranging from 250 to 1400 m asl (Yukon Ecoregions Working Group 2004: Burn et al. 2015). Precipitation amounts in this region are moderate (300–450 mm), with precipitation mainly falling as rain in summer (Yukon Ecoregions Working Group 2004). Contrastingly, the Selwyn Mountains have been extensively glaciated, most recently during the McConnell Glaciation (20 000 years B.P), and still have local alpine glaciers (Bostock 1966). This recent glaciation results in the high range of elevation in these mountains compared to the Ogilvie Mountains, with local relief ranging from 900 to 1500 m and elevation ranging from 650 to 2200 m asl (Yukon Ecoregions Working Group 2004). Additionally, these mountains receive some of the highest amounts of precipitation in Yukon outside of the Pacific Maritime region (600–700 mm) (Yukon Ecoregions Working Group 2004). This heavy amount of snowfall prevents the establishment of continuous permafrost in this region. Large accumulations of glacial sediments are only present at the bottom of major valleys while the upper slopes and smaller valleys are composed of Holocene colluvium. Lastly, this region is expected to have low to moderate segregated ice and negligible wedge ice (O'Neill et al. 2019*a*).

Valley DS is the southernmost site in the Ogilvie Mountains located about 43 km south of the Engineer Creek Territorial Campground. It is an east-facing valley, which is treed on one slope (south facing) and treeless on the other slope (north facing) (Table 1 and Fig. 2).

Valley DS has an elevation difference from the valley floor to the highest ridge of about 700 m and the annual mean air temperature (AMAT) measured at the valley floor was −6.2 °C from 2018 to 2021. Mean monthly SLRs in the valley are strongly inverted during the winter and normal during the summer, resulting in an inverted annual SLR on the treed side of the valley and a slightly less inverted SLR on the treeless side (Noad and Bonnaventure 2022). The valley is considered to be underlain by continuous permafrost (Heginbottom 1995).

Valley DN is the northernmost site and despite being only 10 km away from Valley DS is quite different in terms of vegetation. Valley DN is a treeless valley, with vegetation only consisting of moss and lichen on the valley floor with a few scattered shrubs and scree slopes (Table 1 and Fig. 2). This valley has a north facing aspect. The elevation difference in this valley is 520 m with an AMAT of −4.4 °C (2018–2021) at the valley floor. As with Valley DS mean monthly SLRs are strongly inverted during winter and normal during the summer. The annual SLR in this valley is also inverted (more inverted on the west facing slope than the east) but is not as strong as in Valley DS (Noad and Bonnaventure 2022). This valley is also considered to be in the continuous permafrost zone (Heginbottom 1995).

Mile 222 Valley is located on the North Canol Highway near the Yukon/Northwest Territories boarder in a wide valley. The dominant vegetation is dwarf birch in the lower portions of the valley transitioning into predominately mosses and lichens at higher elevations (Table 1 and Fig. 2). AMAT in the valley bottom is −6.5 °C (2016–2021) and the valley has an elevation difference of about 570 m. Monthly SLRs were generally inverted during winter and normal during the sum-

Fig. 2. Site photos for each of the four valleys. (A) Photo facing southeast at Valley Dempster South (Valley DS) showing the treed and treeless slopes of the valley, taken on 14 August 2018. (B) Photo facing south at Valley Dempster North (Valley DN) showing the limited vegetation in the valley bottom and bare slopes, taken on 14 August 2018. (C) Photo facing southeast at Valley Mile 222 (Valley M222) showing the shrub dominant vegetation and limited relief, taken on 17 August 2019. (D) Photo facing southwest of Valley MacMillan Transect South (Valley MTS), showing the forested valley bottom and lower slope transitioning to alpine tundra, taken on 22 August 2019. Photo credit: Madeleine Garibaldi.

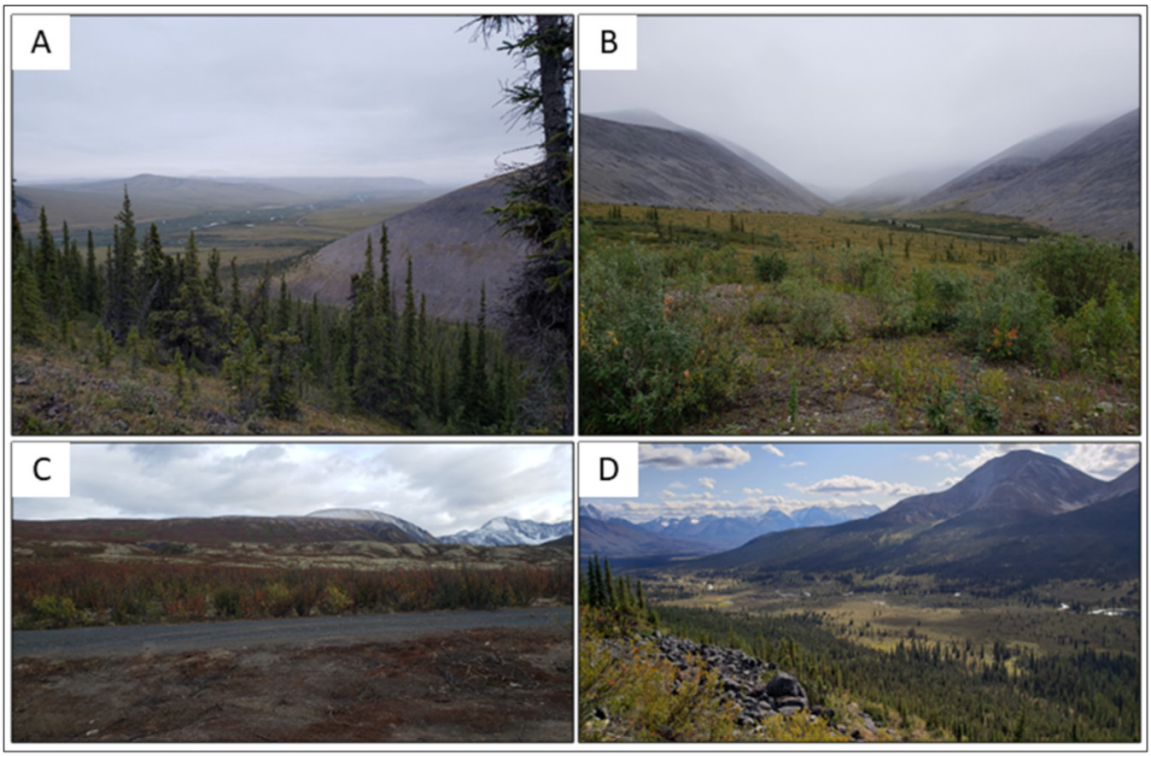

mer; however, the annual SLR in this environment fluctuated between inverted and normal depending on the year. The average SLR in the lower portion of the valley is inverted (<1361 m), while the average SLR at higher elevations is normal. This valley is considered to be underlain by extensive discontinuous permafrost (Heginbottom 1995).

Valley MTS is located along the North Canol and is the southernmost site. This site has the largest elevation difference of the study areas (about 805 m) and is comprised of one treed south-east facing slope (Table 1 and Fig. 2). Above treeline, vegetation is mainly alpine tundra consisting of moss and lichen and scree slopes. The AMAT for this site is −5.9 °C (2019–2021) in the valley bottom, and SLR is inverted below treeline annually and is normal above treeline annually. This valley is also deemed to be in the extensive discontinuous permafrost zone (Heginbottom 1995).

3. Methods

3.1. Site selection and data collection

3.1.1. Air temperature stations

Each valley was equipped with at least three air, ground surface, and ground temperature at depth stations recording temperature bi-hourly (on even hours) (Fig. 3). Air temperature was measured about 1.5 m above the ground surface in a radiation shield (Onset RS1) with a Hobo U23-002 (±0.25 °C accuracy, 0.04 °C resolution) thermistor. At newer sites, a Hobo U23-001 (±0.25 °C accuracy, 0.04 °C resolution) was used. Ground surface temperature was measured using a Hobo U23-002 internal thermistor buried 2–5 cm below the ground surface (under any surface vegetation cover), while ground temperature at depth was measured using the external thermistor located at the depth of the frost table at most sites. Exceptions to this were mainly sites located on exposed rocky substrate or scree. Although these sensors were placed at different depths, they allowed for the estimation of the relative thermal conductivity at each site. Additionally, at sites where the depth sensor is shallow and/or not at the bottom of the active layer the substrate is mainly coarse rock or bedrock. Additional information on the locations of the stations within the valley, the ground sensor depth and the installation year can be found in Fig. 3 and in Table S1 in the supplemental data.

3.1.2. Ground temperature nodes

Sites in each valley were selected to maximize the heterogeneity in ground surface temperature conditions sampled. To do this, variables derived from a Digital Elevation

Fig. 3. Locations of ground surface temperature stations, air temperature stations, and the modelling area for (A) Valley Dempster South (Valley DS), (B) Valley Dempster North (Valley DN), (C) Valley Mile 222 (Valley M222), and (D) Valley MacMillan Transect South (Valley MTS). Colours for the air temperature stations indicate the year of installation. Base layer from DigitalGlobe Inc. (Imagery © [2017]). Contains information licenced under the Open Government Licence—Canada.

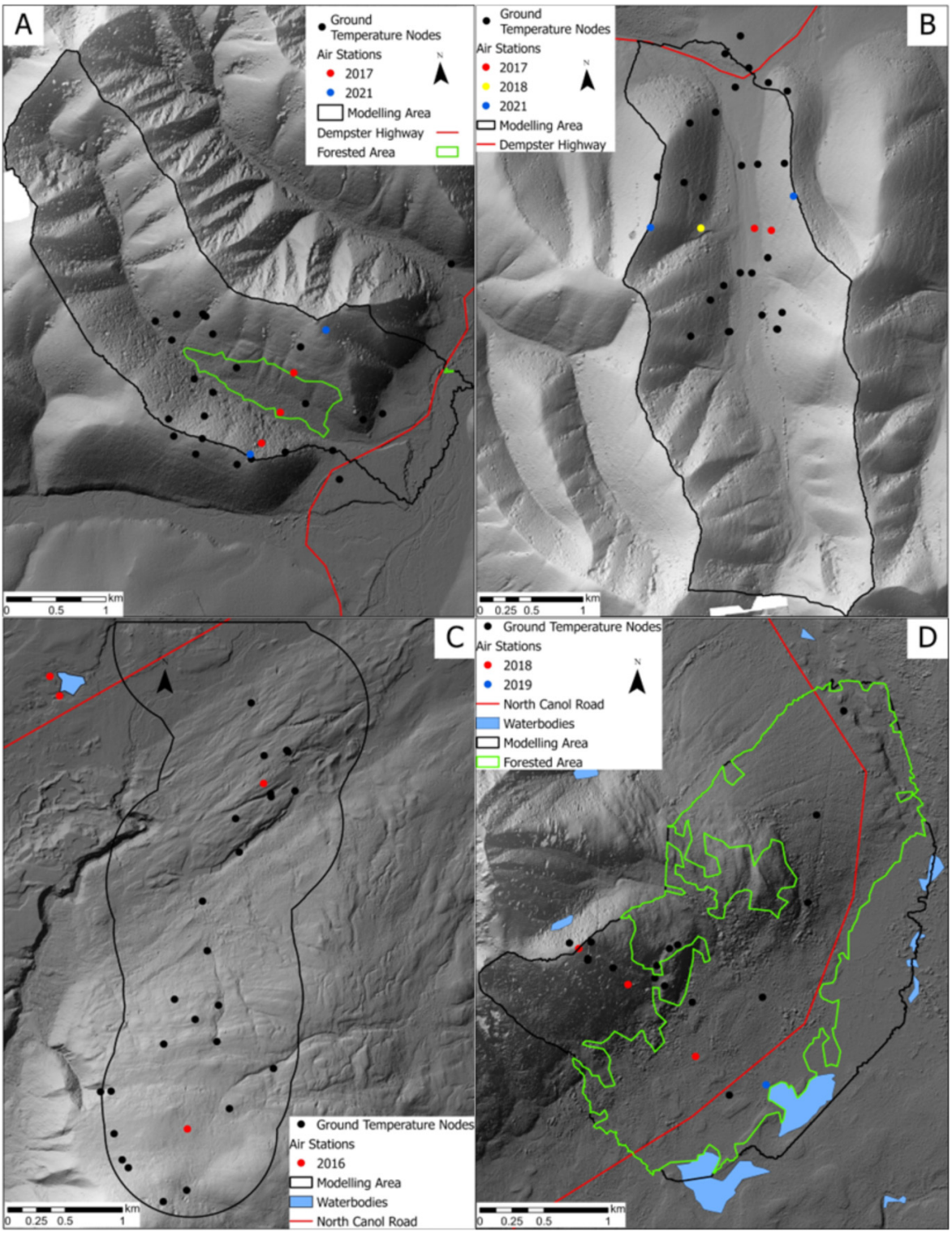

Model (DEM) in ArcGIS including topographic position index (TPI), potential incoming solar radiation (PISR), aspect, slope, and elevation were used. The 2 m spatial resolution elevation models for each valley were derived from GeoEye optical imagery (Imagery © [2017] DigitalGlobe, Inc.). The Polar Geospatial Center at the University of Minnesota produced the surface model through surface extraction with TIN-based search and space minimization (SETSM) algorithm (Noh and Howat

Fig. 4. Schematic of the modelling process for the measured scenario using the measured inverted surface lapse rates (SLRs) and the theoretical scenario using the normal standard environmental SLR (−6.5 °C km^{-1}). AMAT, annual mean air temperature; DEM, Digital Elevation Model; FDD, freezing degree days; TDD, thawing degree days; PISR, potential incoming solar radiation; AMGT, annual mean ground temperature; TWI, topographic wetness index.

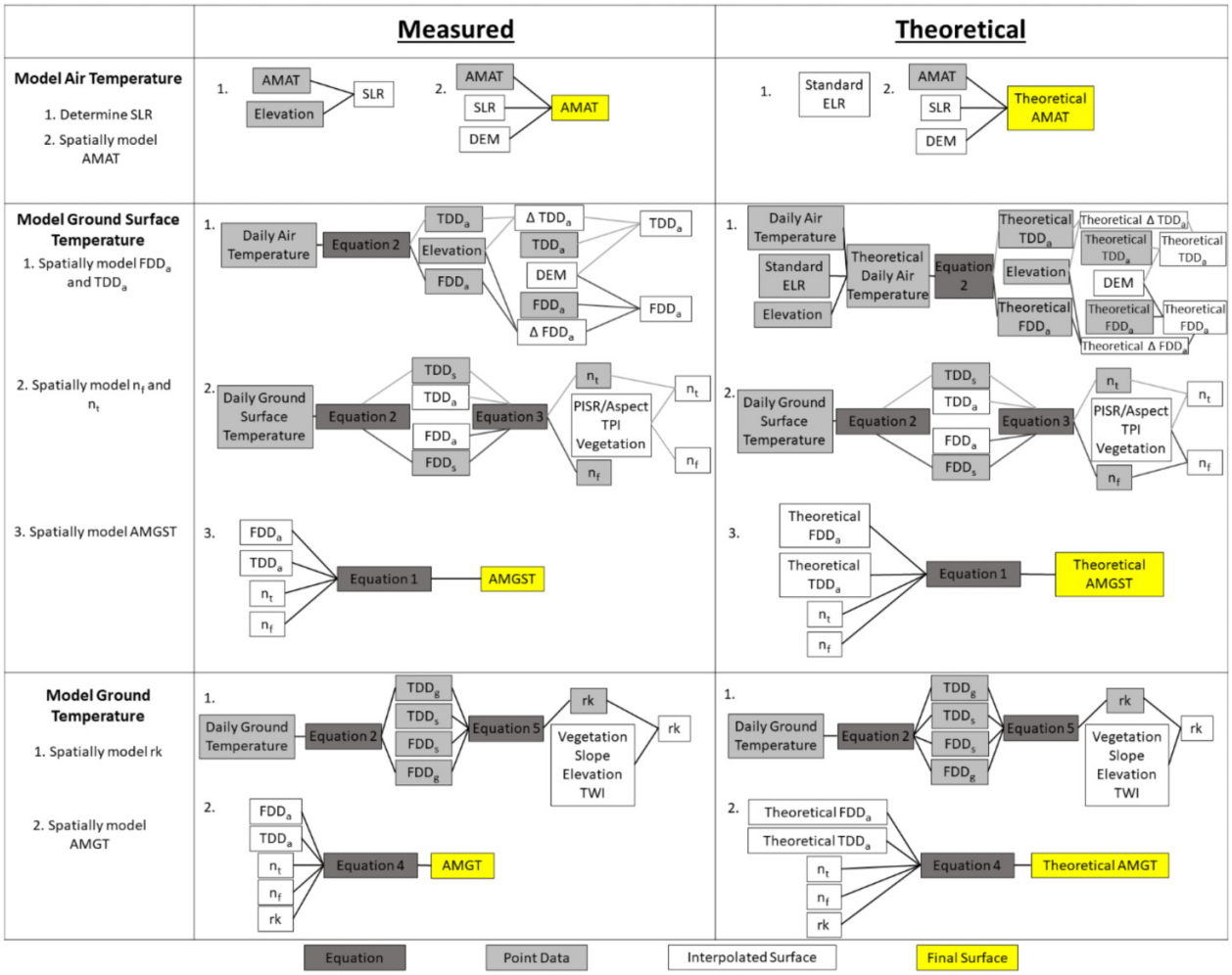

2017). Twenty-five sites in each valley were then selected to sample the spread of topographic and vegetation heterogeneity in each valley, accounting for accessibility (proximity to the existing stations and the road). Some additional sites were added in the field based on in situ observations of the topographic conditions. For sampling, Hobo pendant loggers (±0.53 °C accuracy, 0.14 °C resolution) were selected as they are relatively inexpensive, robust and have had a good success and recovery rate in other locations (Garibaldi et al. 2021; Vegter et al. 2024). Loggers were buried 2–5 cm below the ground surface, including any vegetation cover, and recorded temperature at an hourly interval.

3.2. Data analysis and modelling

Two scenarios were used to model the air and ground thermal regime in each valley, one following the measured inverted annual SLR (referred to subsequently as the measured model) and the second following the normal standard environmental SLR (−6.5 °C km^{-1}), referred to subsequently as the theoretical model. The normal standard environmental SLR is the theoretical free air lapse rate of mixed (dry-wet) air and is considered to be the average SLR across the lower troposphere at any time. Although environmental SLRs in mountains may differ from this standard (even without inversions) depending on air temperature, moisture content, and solar radiation, the standard SLR was used as there is little data on normal environmental SLRs in comparable mountain environments (Barry 2008). The parameters, equations, and steps used in the modelling process are shown in Fig. 4, and additional details on each step are given in the following sections.

3.2.1. AMAT model creation

To create spatial models for air temperature, SLRs were calculated using the daily average temperatures recorded at each station and the elevation. The daily SLRs were then calculated following the formula for the slope of a line to determine the linear relation between air temperature and elevation. The daily averages for 1 August to 31 July of the subsequent year were then averaged to get the annual SLR. The

year was divided from 1 August to 31 July to keep the period for each valley the same and keep the freezing season intact. Due to differences in data collection time periods, SLRs for certain locations and for years outside of the study duration were assumed to be the same as those during the modelling time period. Spatial models for AMAT were then created using the measured SLR, measured AMAT, and the valley DEMs for the measured scenario and substituting in the standard environmental SLR for the theoretical.

3.2.2. AMGST model creation

The annual mean ground surface temperature (AMGST) models were created following a modified temperature at top of permafrost (TTOP) model equation, which removes the thermal conductivity parameter (eq. 1) (Garibaldi et al. 2021).

$$\text{AMGST} = \frac{(n_t * \text{TDD}_a) - (n_f * \text{FDD}_a)}{P} \quad (1)$$

where FDD_a and TDD_a are freezing and thawing degree days in the air, *n*-factors (ratios of ground surface to air temperature) represent the freezing (n_f) and thawing (n_t) surface offsets, and *P* is the period (typically 365 days). The methods and equations to calculate each of these parameters at point locations and the interpolation process to create the spatial models for each are shown in Fig. 4 and further details are discussed in the following sections.

3.2.2.1. *Spatially modelling FDD_a and TDD_a*

For each air temperature station, freezing degree days (FDD) and thawing degree days (TDD) were calculated for each year (eq. 2) (Smith and Riseborough 2002).

$$\text{FDD} = |\Sigma_1^P T|,\ T < 0 \quad (2)$$
$$\text{TDD} = |\Sigma_1^P T|,\ T > 0$$

where *T* is the daily average temperature and *P* is the period. Using this equation FDD and TDD can be calculated for air (a), ground surface (s), and ground (g). As with AMAT, the degree-days were calculated using a split calendar year (1 August to 31 July).

For the measured scenario, the relation between degree days and elevation was determined using the same method as the SLRs. These relations, in conjunction with the measured FDD_a and TDD_a at the lowest station and the DEM for each valley, were used to create the spatial models for measured FDD_a and TDD_a. For the theoretical scenario, the daily average air temperatures at the lowest stations were reduced by 6.5 °C km^{-1} to the elevation of the middle station. These theoretical daily average air temperatures were then used to calculate the theoretical FDD_a and TDD_a at the middle station. These theoretical values, in addition to the measured values at the lowest station, and the elevation difference were used to determine the theoretical change in FDD_a and TDD_a with elevation in the lower portions of the valleys. This was repeated for the middle to upper stations. The spatial models for the theoretical FDD_a and TDD_a were then created using the theoretical change in FDD_a and TDD_a with elevation, the measured FDD_a and TDD_a at the stations, and the DEM for each valley.

3.2.2.2. *Spatially modelling n-factors*

n-factors for each site were calculated following eq. 3 using the spatial models for measured FDD_a and TDD_a and the measured ground surface freezing and thawing degree days (FDD_s) and (TDD_s) at each site.

$$n_f = \frac{\text{FDD}_s}{\text{FDD}_a} \quad \text{and} \quad n_t = \frac{\text{TDD}_s}{\text{TDD}_a} \quad (3)$$

To allow for the creation of spatial maps for the *n*-factors, aspect and/or potential incoming solar radiation (PISR), topographic position index (TPI), and vegetation were used to relate topographic or spatial biological variables to the measured *n*-factors. These variables were used as all have been shown to influence the distribution of thawing and freezing surface offsets (Smith and Riseborough 2002; Lacelle et al. 2016; Obu et al. 2019; Garibaldi et al. 2021; Garibaldi et al. 2022). PISR was derived using the Area Solar Radiation tool (ArcGIS Pro) for 15 May to 30 September 2018, with a sky size of 400 and 16 Zenith/Azimuth division (Bonnaventure and Lewkowicz 2011). The default was used for the remaining inputs. TPI compares elevation of each cell to the mean elevation of a user-specified neighborhood (Jenness 2006). For each valley, a 200 × 200 m window was utilized. Finally, a vegetation class was determined from a 30 m vegetation inventory feature layer (Government of Canada 2015).

These relations between the *n*-factors and the topographic and environmental characteristics of a site were then used to create the spatial *n*-factor models using Empirical Bayesian Kriging (EBK) in ArcGIS Pro. EBK is a combination of ordinary least-squared regression and simple kriging, where the dependent variable is predicted through the sum of the average value and an error term. The average value is determined from the regression equation (weighted sum of the explanatory variables), and the error term is determined from a semivariogram or covariance model. The combination of regression and kriging in EBK allows for more accurate predictions than either method individually. Several iterations of EBK for each *n*-factor in each valley were run to determine the combination of input variables with the lowest error. Predicted values for n_f and n_t were capped for each EBK model to limit unreasonable predictions. These capping values were determined for each valley and parameter based on the measured values and the known general limitation of each parameter. As a result, n_f was capped between 0.0 and 1.0, while n_t was capped between 0.0 and 2.0. Due to the narrower range, n_f surfaces required more capping than n_t. For each valley, capping was only required for a small portion of the valley and generally was required in locations where TPI and PISR values were outside of the range sampled through the ground sensor network. The spatial distribution for the *n*-factors for each valley can be found in the supplemental data (Figs. S1–4).

Finally, the measured and theoretical AMGST models were created by combining all the parameter surfaces into eq. 1. For the measured model, the measured FDD_a and TDD_a were

Table 2. Annual mean air temperature (AMAT) for the modelling period for both the measured data and from ClimateNA, climate normal (1981–2010) from ClimateNA, annual average surface lapse rates (SLR), and the elevation difference between air stations for each valley.

Valley	AMAT (2019–2021)	ClimateNA AMAT (2019–2021)	Climate normal (1981–2010)	Lower SLR (°C km^{-1})	Upper SLR (°C km^{-1})
Valley DS	−7.4	−6.1	−6.2	11.7 (Treed)	− 0.9 (Treed)
				8.0 (Treeless)	0.5 (Treeless)
Valley DN	−5.4	−6.9	−7.0	3.5 (E facing)	− 0.1 (E facing)
				7.1 (W facing)	1.3 (W facing)
Valley M222	−6.1	−6.0	−6.3	5.9	− 2.7
Valley MTS	−5.9	−5.6	−5.6	10.6	− 5.1

Note: ClimateNA data from https://climatena.ca/mapVersion (Wang et al. 2016). Valley DS, Valley Dempster South; Valley DN, Valley Dempster North; Valley M222, Valley Mile 222; Valley MTS, Valley MacMillan Transect South.

used, while the theoretical AMGST model utilized the theoretical FDD_a and TDD_a. For both scenarios, the same *n*-factor models were used.

3.2.3. AMGT model creation

The TTOP model (eq. 4) was used to spatially model annual mean ground temperature (AMGT) at the base of the active layer (or seasonally frozen surface layer) due to its simplicity and transferability between locations (Smith and Riseborough 2002).

$$\text{TTOP} = \frac{(rk * n_t * \text{TDD}_a) - (n_f * \text{FDD}_a)}{P} \quad \text{for TTOP} \leq 0$$

$$\text{TTOP} = \frac{(n_t * \text{TDD}_a) - \left(\frac{1}{rk} * n_f * \text{FDD}_a\right)}{P} \quad \text{for TTOP} > 0 \tag{4}$$

where *rk* is the differential thermal conductivity between the frozen and thawed substrate and the other parameters are the same as those defined in eq. 1. Since the TTOP model assumes equilibrium conditions, the AMATs for each year in each valley were assessed to see how close they were to the 1981–2010 climate normal. This was done using ClimateNA to determine the climate normal at the lowest air station in each valley (Wang et al. 2016).

Spatial models for the remaining parameter, rk, were created for each valley using a combination of calculated values from the ground surface and depth temperatures (recorded at each air station) and inferences based on topographic and landcover characteristics (Table S2 and Figs. S1–4). For each valley, rk values for every air station were calculated using FDD_s, TDD_s, and freezing and thawing degree days in the ground at depth (FDD_g and TDD_g) (eq. 5) (modified from Way and Lewkowicz 2018).

$$rk = \frac{\text{FDD}_s + (\text{TDD}_g - \text{FDD}_g)}{\text{TDD}_s} \tag{5}$$

FDD_g and TDD_g were calculated using the daily average ground temperatures at depth for each station with a ground depth sensor and eq. 2. The resulting rk values for each station were then assigned to the vegetation class in which the air station was located to allow for spatial modelling. Some air stations located in the same vegetation class had differing calculated rk values. To account for this, elevation, slope, and topographic wetness index (TWI) were also used to infer the spatial distribution of rk. Slope was calculated using the DEM and ArcGIS Pro. TWI is an index that describes the tendency of an area to accumulate water and is derived using the upslope contributing area and slope. To determine the upslope contributing area, several hydrology tools from the Spatial Analyst toolbox in ArcGIS Pro were utilized, including Flow Direction and Flow Accumulation.

The parameter surfaces were then combined using the TTOP model in raster calculator (ArcGIS Pro) (eq. 4). For pixels where TTOP was calculated to be greater than 0 °C, the TTOP model for seasonal frost was used (eq. 4), and the AMGT surfaces were made through the combination of the areas calculated using the TTOP model and the seasonal frost model (Vegter et al. 2024). The AMGT surfaces were then validated against the measured ground temperatures at depth recorded in each valley. Again, for the measured and theoretical scenarios measured FDD_a and TDD_a or theoretical FDD_a and TDD_a were used.

4. Results

4.1. SLRS and AMAT comparison to climate normal

The measured air temperatures in all four valleys (in addition to the ClimateNA predicted air temperatures) during the two years were similar to that of the 1981–2010 climate normal for each valley (Table 2) (Wang et al. 2016). Both Valley M222 and Valley MTS were most similar to the respective climate normals, while Valley DS and DN showed a greater difference. However, due to the remote nature of these valleys and their complex topography, it is possible that even the 1981–2010 climate normal may not be representative. All four valleys experienced substantial winter inversions resulting in an inverted annual SLR in at least the lower portion of the valley (Table 2). In Valley DS and Valley DN, the inverted annual SLRs on one slope extended above the mid-elevation station to the ridge top (treeless and west-facing slopes, respectively), although they were substantially less inverted than those in the valley bottom. On the other slope in

Table 3. Average annual mean air temperature (AMAT), annual mean ground surface temperature (AMGST), and annual mean ground temperature (AMGT) across each valley and the percentage of the valley underlain by near surface permafrost (NSP) for the measured inverted surface lapse rate (SLR) and for the assumption of a normal environmental SLR.

	AMAT (°C)		AMGST (°C)		AMGT (°C)		NSP (%)	
	Measured	Theoretical	Measured	Theoretical	Measured	Theoretical	Measured	Theoretical
Valley DS	−6.4	−8.8	−1.4	−3.3	−1.6	−3.5	80	88
Valley DN	−5.1	−6.7	−1.8	−2.8	−2.1	−3.1	99	100
Valley M222	−6.2	−7.2	0.4	0.2	0.3	−0.3	33	51
Valley MTS	−5.1	−6.6	0.9	0.3	−0.3	−0.8	61	96

Note: Valley DS, Valley Dempster South; Valley DN, Valley Dempster North; Valley M222, Valley Mile 222; Valley MTS, Valley MacMillan Transect South.

Table 4. Root means square error (RMSE) for the testing data for the *n*-factor, annual mean ground surface temperature (AMGST), and annual mean ground temperature (AMGT) models.

	n_f	n_t	AMGST (°C)	AMGT (°C)
Valley DS	0.08 (0.27)	0.21 (0.84)	1.1 (0.2)	0.9 (−0.1)
Valley DN	0.13 (0.61)	0.20 (1.00)	0.4 (−2.2)	0.7 (−2.9)
Valley M222	0.10 (0.24)	0.15 (1.00)	1.1 (0.1)	1.9 (0.7)
MTS Valley	0.08 (0.16)	0.09 (0.82)	0.5 (1.3)	0.5 (0.4)

Note: The average value for the measured parameter is shown in parentheses. Valley DS, Valley Dempster South; Valley DN, Valley Dempster North; Valley M222, Valley Mile 222; Valley MTS, Valley MacMillan Transect South.

these valleys, the SLR was marginally normal above the mid-elevation station. In Valley M222 and Valley MTS, the annual inverted SLRs were only present below the mid-elevation station, with the annual SLR reverting to normal at high elevations.

4.2. Modelled temperatures

For all four valleys, air, ground surface, and ground temperatures showed considerable spatial variability. Air temperature for the measured scenario in all four valleys was coldest at the valley bottom and warmest at either mid or high elevations due to the presence of the inverted SLRs during winter. The topographic pattern of air temperature, however, was not always replicated in the ground surface temperature and ground temperature distribution. When following the theoretical scenario, AMAT, AMGST, and AMGT were all modelled to be colder than the measured scenario especially at high elevations (Table 3). This assumption led to an overestimation of the area of each valley underlain by near surface permafrost (NSP). Root mean square errors (RMSEs) for TTOP model parameters and the annual ground temperatures were relatively low (Table 4).

In Valley DS, the spatial distribution of AMAT for the measured and theoretical scenarios was reversed (Figs. 5A and 5B).

This led to differences in AMAT of up to 6 °C between the two scenarios (Fig. 5C). However, despite the differences in AMAT, the spatial distribution of modelled AMGST, was similar (Figs. 5D and 5E). The exception to this was the magnitude of AMGST that was different especially at high elevations (up to 6.0 °C) (Fig. 5F). The spatial distribution pattern of AMGT was also similar between the two scenarios, with the coldest temperatures at high and low elevations (Figs. 5G and 5H). However, the magnitudes of AMGT were different especially at high elevations (up to 6.8 °C), and the percentage of the valley underlain by NSP also differed slightly (Fig. 5I).

In Valley DN, modelled AMATs for the measured and theoretical scenarios were also reversed (Figs. 6A and 6B).

The largest discrepancy in AMAT between the two scenarios occurred at high elevations (up to 4.5 °C) (Fig. 6C). The spatial distribution pattern of AMGST was similar for the two scenarios with the coldest modelled located at higher elevations and on exposed ridges. The warmest AMGSTs were predicted in a disturbance dominated by shrubs in the valley bottom and in incised channels along the slopes (Figs. 6D and 6E). However, AMGST between the two scenarios showed discrepancies up to 4.5 °C at high elevations (Fig. 6F). For both scenarios, the spatial distribution of AMGT was similar to AMGST; however, the coldest AMGTs for the measured scenario were also in the valley bottom (Figs. 6G and 6H). The greatest difference in AMGT between the two scenarios was found at high elevations (up to 4.5 °C) (Fig. 6I). NSP was modelled to underlay almost all of the valley in both scenarios.

In Valley M222, differences in the spatial distribution of AMAT following the two scenarios were more complex than for the previous two valleys. For the measured scenario, the warmest air temperatures were predicted to be at mid elevations with relatively cold temperatures found in the valley bottom and at higher elevations (Fig. 7A), while for the theoretical scenario the warmest temperatures were expected at the valley bottom and the coldest temperatures were expected at higher elevations (Fig. 7B).

As a result of the different spatial distributions, the greatest difference between the two models was at the highest elevations. Here, AMAT from the measured scenario was up to 2.8 °C warmer (Fig. 7C). The spatial distribution of AMGST between the two scenarios is similar with the largest difference at high elevations (up to 1.8 °C) (Figs. 7D–7F). For both

Fig. 5. Valley Dempster South (Valley DS) annual mean air temperature (AMAT) models for the (A) measured scenario, (B) theoretical scenario, and (C) difference between the two scenarios. Valley DS annual mean ground surface temperature (AMGST) models for the (D) measured scenario, (E) theoretical scenario, and (F) difference between both scenarios. Valley DS annual mean ground temperature (AMGT) models for the (G) measured scenario, (H) theoretical scenario, (I) difference between the two scenarios. For the difference figures, negative values indicate temperatures for the measured scenario are colder than in the theoretical scenario, while positive values indicate the temperatures for the measured scenario are warmer than the theoretical scenario. Base layer from DigitalGlobe Inc. (Imagery © [2017]).

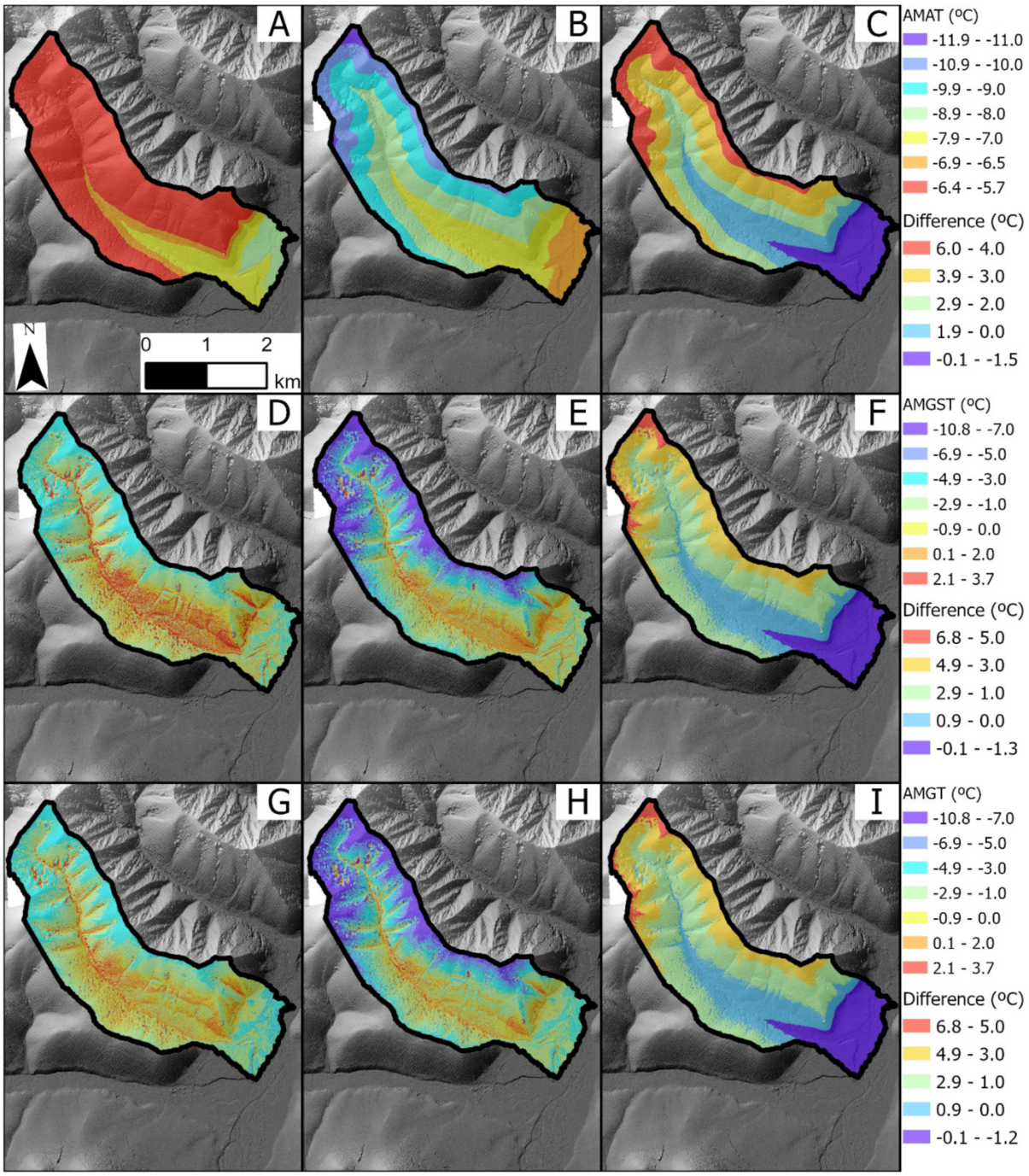

scenarios, the spatial distribution of AMGT was similar to AMGST with the coldest AMGTs predicted on exposed ridges and steep slopes, especially at high elevations (Figs. 7G and 7H). The differences between the two scenarios were greatest at high elevations (up to 2.6 °C), and there was a large discrepancy in the area of the valley expected to be underlain by NSP (Fig. 7I).

In Valley MTS, AMAT for the measured scenario were predicted to be coldest in the valley bottom and warmed moving upslope until reaching a maximum around treeline (Fig. 8A).

Fig. 6. Valley Dempster North (Valley DN) annual mean air temperature (AMAT) models for the (A) measured scenario, (B) theoretical scenario, and (C) difference between the two scenarios. Valley DN annual mean ground surface temperature (AMGST) models for the (D) measured scenario, (E) theoretical scenario, and (F) difference between both scenarios. Valley DN annual mean ground temperature (AMGT) models for the (G) measured scenario, (H) theoretical scenario, and (I) difference between the two scenarios. For the difference figures, negative values indicate temperatures for the measured scenario are colder than in the theoretical scenario, while positive values indicate the temperatures for the measured scenario are warmer than the theoretical scenario. Base layer from DigitalGlobe Inc. (Imagery © [2017]).

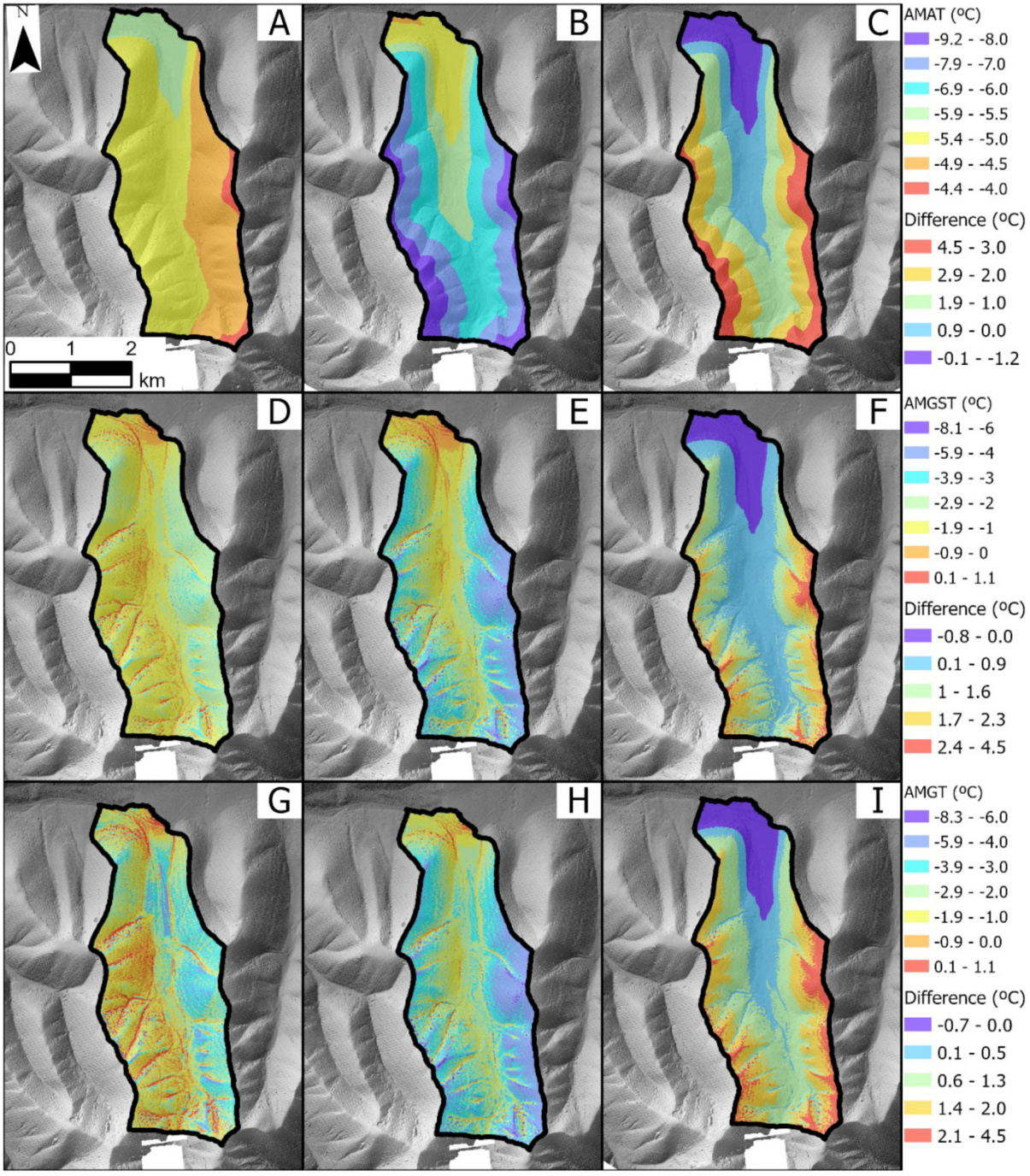

Following the theoretical scenario, the warmest AMATs were predicted in the valley bottom, and the coldest AMATs were predicted at the highest elevations (Fig. 8B). The greatest difference between the two scenarios occurred at high elevations (up to 4.8 °C) (Fig. 8C). Unlike the previous valleys, the spatial distribution of AMGST in Valley MTS between the two scenarios was different, especially at mid to high elevations above and around treeline (up to 2.5 °C) (Figs. 8D–8F). The spatial distribution of AMGT closely matched the spatial distribution of AMGST for each scenario at mid to high eleva-

Fig. 7. Valley Mile 222 (Valley M222) annual mean air temperature (AMAT) models for the (A) measured scenario, (B) theoretical scenario, and (C) difference between the two scenarios. Valley M222 annual mean ground surface temperature (AMGST) models for the (D) measured scenario, (E) theoretical scenario, and (F) difference between both scenarios. Valley M222 annual mean ground temperature (AMGT) models for the (G) measured scenario, (H) theoretical scenario, and (I) difference between the two scenarios. For the difference figures, negative values indicate temperatures for the measured scenario are colder than in the theoretical scenario, while positive values indicate the temperatures for the measured scenario are warmer than the theoretical scenario. Base layer from DigitalGlobe Inc. (Imagery © [2017]). Contains information licenced under the Open Government Licence—Canada.

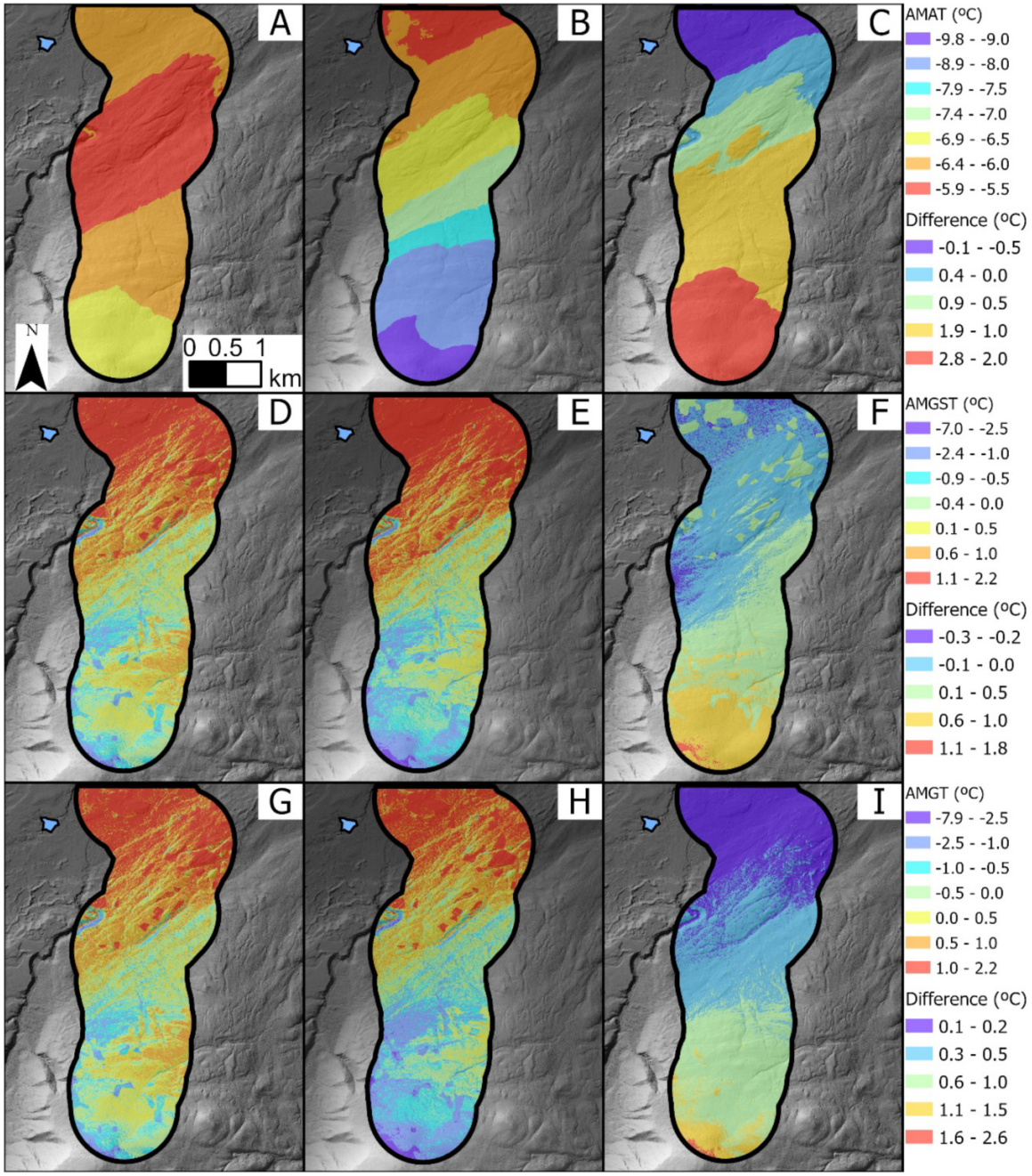

tions (Figs. 8G and 8H). However, at low elevations, there was a large discrepancy where AMGT were modelled to be colder than AMGST. The difference in AMGT between the two scenarios was greatest at high elevations (up to 2.3 °C) where AMGT following the theoretical scenario was predicted to be colder than the measured scenario leading to an overestimation by 35% of the area underlain by NSP (Fig. 8I).

4.3. Comparison to regional permafrost probability model

Average permafrost probability from a regional model (Bonnaventure et al. 2012) for each valley (Figs. 9A, 9C, 9E, and 9G) was compared to the percentage of the valley underlain by permafrost in the local models (Figs. 9B, 9D, 9F, and 9H). The permafrost probability and permafrost presence

Fig. 8. Valley MacMillan Transect South (Valley MTS) annual mean air temperature (AMAT) models for the (A) measured scenario, (B) theoretical scenario, and (C) difference between the two scenarios. Valley MTS annual mean ground surface temperature (AMGST) models for the (D) measured scenario, (E) theoretical scenario, and (F) difference between both scenarios. Valley MTS annual mean ground temperature (AMGT) models for the (G) measured scenario, (H) theoretical scenario, and (I) difference between the two scenarios. For the difference figures, negative values indicate temperatures for the measured scenario are colder than in the theoretical scenario, while positive values indicate the temperatures for the measured scenario are warmer than the theoretical scenario. Base layer from DigitalGlobe Inc. (Imagery © [2017]). Contains information licensed under the Open Government Licence—Canada.

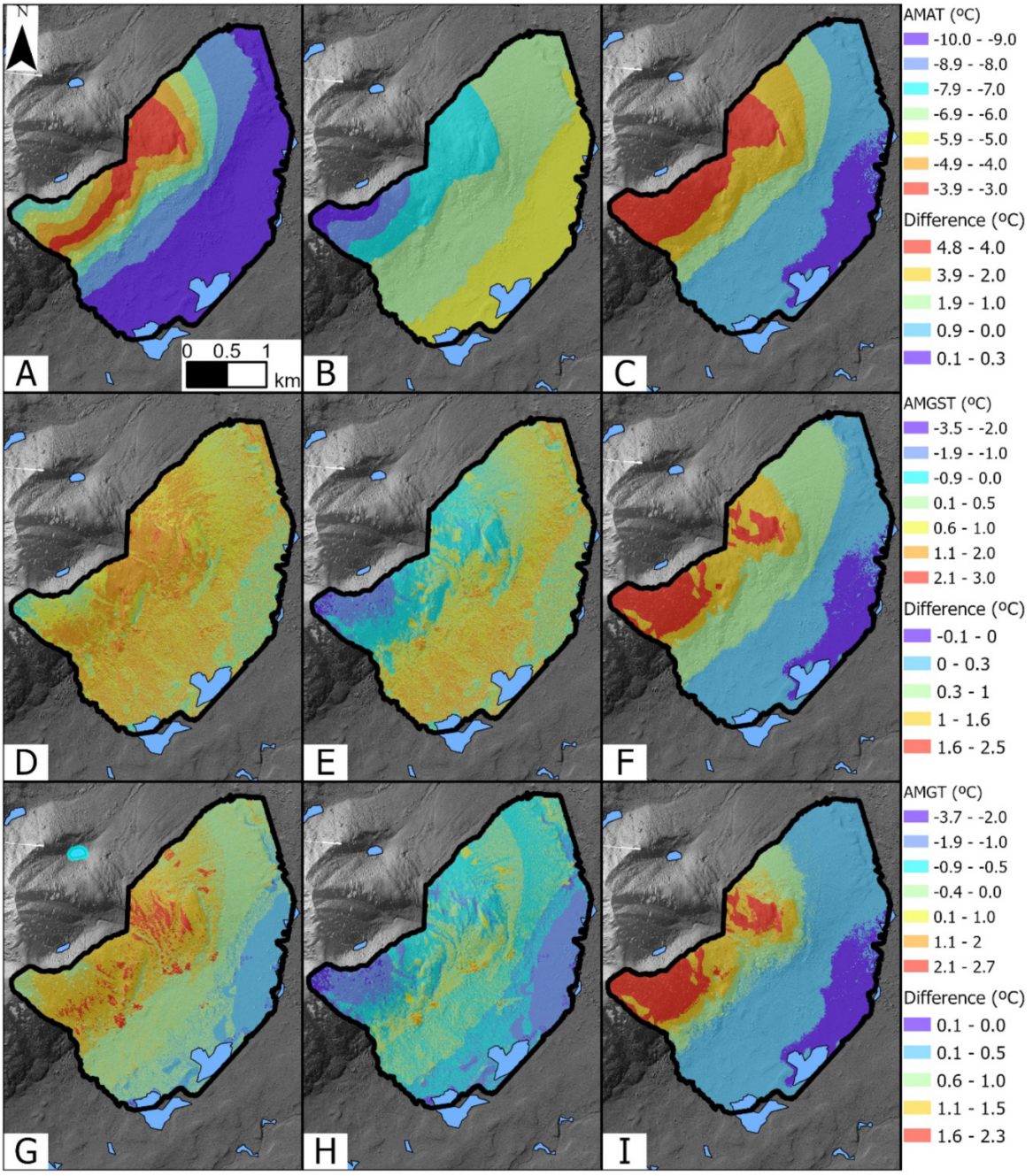

were closest in Valley DS where average permafrost probability was 71%, while NSP was expected to underlie 80% of the valley.

Valley DS was the only valley in which the probability model predicted a lower percentage of permafrost than the local AMGT model. The regional model, however, did not agree as well in Valley DN with average permafrost probability of 80% and a predicted NSP of 99%.

The probability model had the largest discrepancy in Valley M222 where average probability was 77%, while only 33% of the valley had predicted NSP. Finally, in the Valley MTS, both models captured the lack of or low probability around

Fig. 9. Valley Dempster South (Valley DS) (A) permafrost probability and (B) near surface permafrost (NSP) presence and absence. Valley Dempster North (Valley DN) (C) permafrost probability and (D) NSP presence and absence. Valley Mile 222 (Valley M222) (E) permafrost probability and (F) NSP presence and absence. Valley MacMillan Transect South (Valley MTS) (G) Permafrost probability and (H) NSP presence and absence. Base layer from DigitalGlobe Inc. (Imagery © [2017]).

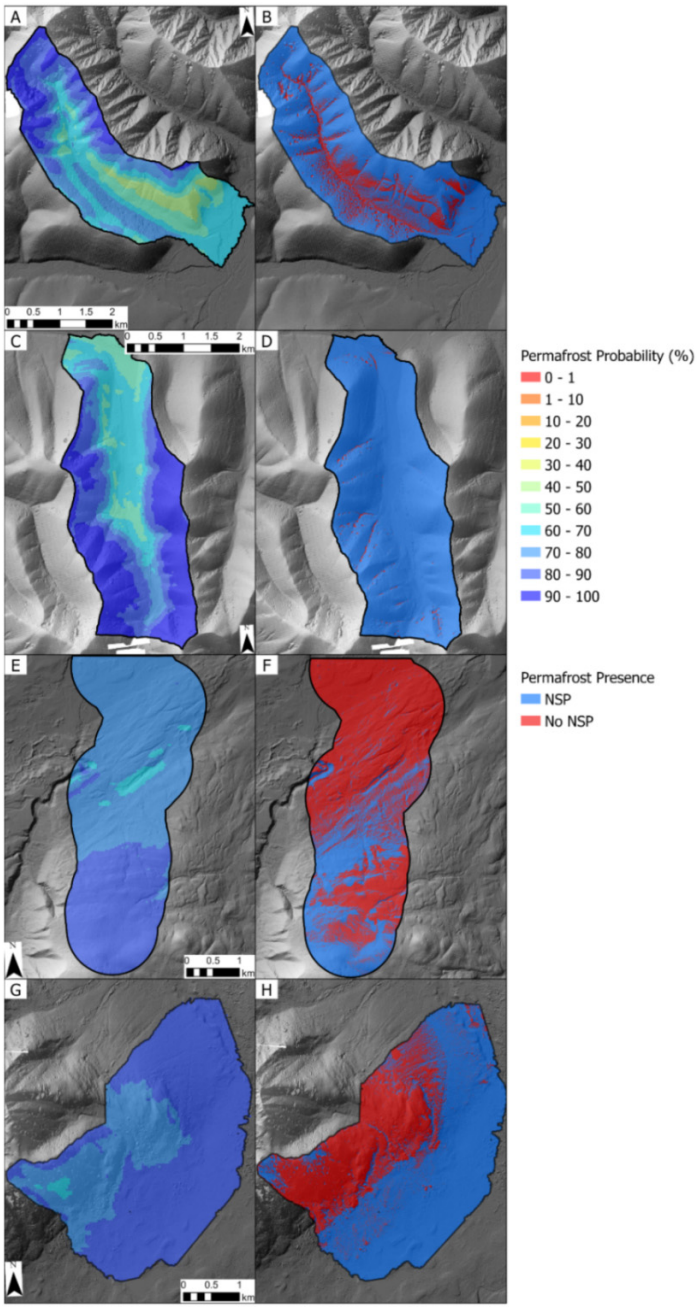

the treeline and the presence or high probability in the valley bottom. However, average permafrost probability was higher than the area underlain by NSP (80% and 61%, respectively). Overall, the regional model agreed with most of the local AMGT models capturing the general patterns of permafrost distribution.

5. Discussion

5.1. Errors and locations of uncertainty

Although the RMSEs for the AMGST and AMGT surfaces are comparable to those from previous modelling studies (Obu et al. 2019; Garibaldi et al. 2021), there were a few locations within the valleys that may have larger errors. In Valley DS and Valley DN, most of the ground surface sensors were located near the front of the valley. As a result, deeper parts of the valley were not sampled and therefore were not included in the model creation or testing. Additionally, since these parts of the valley were outside of the sampled area, they were modelled more through extrapolation than interpolation, which often led to unrealistic predictions of n_f and n_t. However, the capping of these unrealistic n-factor values likely limited the error in AMGST and AMGT in these locations.

In Valley M222, the measured scenario predicted the warmest AMGST and AMGT at the valley bottom and the coldest at high elevations. However, the measured values at these sites indicated the opposite, with colder AMGST and AMGT at the valley bottom compared to high elevations. One possible reason for this discrepancy is the assigned rk values. At M222 03, measured rk was calculated to be up to 2.0 for certain years. As rk values in previous literature have been assumed to be equal to or less than 1.0, the maximum rk value used in this modelling was set at 1.0. This may explain why AMGTs were underestimated at this upper elevation site. Finally, another explanation could be the strength of the inverted SLR during the years used in the study. From August 2016 to August 2018, the annual SLRs between the lowest and mid station were much more inverted than during the sampling years (up to 19 °C km^{-1}). This likely resulted in colder AMGST and AMGT at the valley bottom during this time. Additionally, although the model predicts no NSP in the valley bottom, there is evidence of permafrost in this area as there is at least one palsa in the valley bottom. As the AMAT in the valley bottom during the sampling years was representative of the 1981–2010 climate normal, it is possible that the palsa is not in equilibrium with the current climate (Seppälä 1982; Shur and Jorgenson 2007; Mamet et al. 2017).

Finally, in Valley MTS, the locations with the largest uncertainty in predicted AMGST and AMGT are located in portions of the valley bottom and in locations of burnt coniferous forest. First, there are a number of water bodies located at the valley bottom, which extend into the shrubs lining the shores. As a result, certain parts of the valley bottom classified as shrubs may have extremely wet terrain and be underwater for part of the year. This was attempted to be represented by applying a low rk (0.1) to large portions of the lowest elevations in this valley. The advective heat transfer and moderating impacts of the lakes are not directly accounted for in the model and may explain why TDD_a in the lower portion of this valley increased with increasing elevation. Lastly, the vegetation classification did not have a class for burnt coniferous forest even though recently burned areas are present near the modelling area. Measured AMGST at the burned site were up to 3.5 °C warmer than a comparable unburnt site. As a result, any areas of burnt forest are not

accounted for in this model. Although there are limitations to the models in each valley, overall, they are likely representative of the ground thermal conditions in these valleys and show comparable error to other modelling studies with longer measurement records (Obu et al. 2019).

Since the TTOP model is an equilibrium permafrost model, input parameters should be within the climatological normal to accurately predict AMGT. For Valley DN and Valley M222, using a longer data record (5 years) resulted in AMAT with a greater discrepancy from the downscaled climate normal than the two-year record used in this study. For Valley M222, the difference between the 2- and 5-year record compared to the climate normal was minimal (0.24–0.17 °C, respectively). However, for Valley DN, increasing the record length resulted in an overestimation of AMAT in the valley bottom of 2.2 °C rather than 1.6 °C. For Valley DS, using the 5-year data record would have decreased the difference from the climate normal by 0.7 °C. Since the air temperatures were underestimated compared to the climate normal, NSP extent and AMGT may have been overestimated and underestimated, respectively. However, as the purpose of the study was to assess the spatial distribution of the ground thermal regime, the resulting relative distribution of AMGT was likely to be accurate even if the exact magnitude of AMGT is underestimated. Furthermore, as these valleys are located in complex and remote topography, there is little in situ data that can be used to validate the accuracy of the downscaled climate reanalysis data. As a result, it is possible that even these data are not representative of the normal climatic conditions in these valleys (Noad and Bonnaventure 2022).

5.2. Influences on modelled AMGST and AMGT within and between valleys

The spatial models for AMGST and AMGT showed the impact of the temperature inversions, especially when compared to the theoretical scenario assuming normal SLRs. Following the theoretical scenario, AMGSTs at high elevations were expected to be much colder than those predicted using the measured scenario, due to the colder AMAT and the high n_f values (low surface offsets) at these locations (Zhang 2005; Lewkowicz et al. 2012; Bevington and Lewkowicz 2015; Freudiger et al. 2017). This allowed for a more direct impact of the colder air temperatures on the ground surface. The interaction between AMAT and n_f likely explains why Valley M222 and Valley MTS saw limited difference in AMGST between the measured and theoretical scenarios. This may partially be explained by the reversal of the inverted SLR at mid elevations, limiting the difference in AMAT between the two models at this elevation. However, this may also result from the lower maximum n_f values at high elevations in these valleys (0.83 and 0.85) compared to those for Valley DS and Valley DN (1.00), resulting in similar ground surface temperatures despite the difference in air temperature. The lower maximum n_f values in the valleys with warmer AMGSTs aligns with theoretical values for n_f based on both snow depth and MAAT and measured values in frozen and unfrozen terrain (Smith and Riseborough 2002; Karunaratne and Burn 2003; 2004). The lower maximum n_f is also likely a product of the increased snowfall and accumulation in the Selwyn Mountains compared to the Ogilvie Mountains (Yukon Ecoregions Working Group 2004). However, at the highest elevations and most exposed terrain, snow depth is likely to be relatively low. Therefore, another possibility for the lower measured and modelled n_f for the North Canol valleys could be the release of latent heat from the subsurface to the surface longer into the freezing season due to the warmer ground conditions.

The rk values influenced both the difference in AMGT and NSP extent predicted in both scenarios through potential buffering of the ground at depth from differences in AMAT. This resulted in limited difference in AMGT and NSP between the two scenarios, especially in the valley bottoms. Additionally, the thermal conditions of the ground in each valley impacted the discrepancy in NSP between the two scenarios. For Valley DS and Valley DN, the AMGT models showed fairly large differences in average AMGT between the scenarios but limited differences in NSP (8% and 1%, respectively). This is a result of the cold ground thermal conditions, whereby the increase in AMGT for the measured scenario did not result in large portions of the valley transitioning from below 0 °C to above. The ground thermal conditions also explain the large difference in NSP (35%) despite the small difference in AMGT between the two scenarios for Valley MTS. The marginal nature of AMGTs in this valley allowed small differences in AMGT to result in a transition from NSP to seasonal frost. Similarly, at Valley M222, due to the limited amount of marginal NSP (due to the overall lack of permafrost), a large difference in average AMGT between the two scenarios did not result in a large change in NSP (18%).

5.3. Comparison to previous models

5.3.1. Circumpolar models

Based on previous assessments of NSP in Canada, the two Dempster valleys should be classified as continuous permafrost, whereby permafrost underlays 90%–100% of the landscape, and the two North Canol Road valleys should be classified as extensive discontinuous permafrost, 50%–90% (Heginbottom 1995). Valley DN and Valley MTS matched the designations from the circumpolar map. However, Valley DS and Valley M222 did not. This may result from different scales used in the circumpolar map creation, as Valley DS is located on the margin of continuous to discontinuous permafrost, and the remoteness of the region limited data from this area used in the circumpolar map creation. Additionally, as discussed earlier, it is also possible that Valley M222 is out of equilibrium with the current climate. A previous comparison of this circumpolar map to regional models of permafrost probability in Yukon noted that the northern end of the study area was classified as extensive discontinuous, while the regional model classified this area as sporadic (Bonnaventure et al. 2012). This was attributed to the presence of strong inversions in these highly continental locations, resulting in the absence of permafrost around treeline. This may also explain why Valley DS and Valley M222 were assumed to have a greater permafrost extent in the circumpolar model compared to the predictions of this study.

An updated, high-spatial-resolution circumpolar permafrost map also does not correctly classify all four valleys. In this updated circumpolar model, Valley M222 and Valley DN are still classified as extensive discontinuous (Obu et al. 2019). This map does, however, match the classification of Valley DS, mapping it as extensive discontinuous, and is partially correct in the classification of Valley MTS as either sporadic or extensive discontinuous.

5.3.2. Regional Yukon model

The spatial distribution of AMGT closely matches those of previous studies in various parts of Yukon. Both the spatial AMGT models created for the four valleys in this study and a larger regional model for Yukon predict permafrost to be present at both high elevations and at the valley bottom (Bonnaventure et al. 2012; Lewkowicz et al. 2012). This results in no lower elevation limit of permafrost in locations with inverted SLRs, which are generally found in continental mountain regions. However, due to the difference in scale, the distribution of permafrost and AMGT was more complex in each of the valleys than predicted in the regional model. Additionally, assumptions of treeline elevation and a weaker, more uniform SLR assumed for all four valleys contributed to model discrepancies. First, the regional model of permafrost probability (Bonnaventure et al. 2012) assumed a 1 °C km^{-1} inverted SLRs in all four valleys. Second, based on assumptions of treeline, Valley DS, Valley MTS, and Valley M222 were all considered to be partially below treeline, while Valley DN was above treeline entirely. This impacted permafrost probability predictions as inverted SLRs in the regional model were only implemented in valleys with elevations below treeline. The SLRs were also assumed to be normal above treeline. As a result of these assumptions, the regional model's permafrost probability performance varied compared to the permafrost distribution for each of the fine resolution models for the valleys.

In Valley DS, the regional permafrost probability model (Bonnaventure et al. 2012) and the local AMGT model showed the best agreement both in terms of the spatial distribution of permafrost and the percentage of NSP likely present in the valley. This was likely due to this valley adhering to the model assumptions (treeline and forested) and its proximity to one of the training locations (Dawson). There was also good agreement between the regional and local models for Valley MTS in terms of the spatial distribution pattern and the area of the valley predicted to be underlain by permafrost. Again, this is likely a product of correct prediction of treeline for the valley. However, there was a larger difference for this valley than Valley DS, possibly since it was farther away from the sampling locations. Although the SLR used in the regional model vastly underestimated the strength of the inversions present in these valleys, it did not largely impact the permafrost probability prediction. This is potentially because of the mature ecosystem present in these valleys limiting the impact of air temperature on permafrost presence, especially in the valley bottom (Shur and Jorgenson 2007). Additionally, as the regional model assessed permafrost probability rather than strict presence or absence (as in the local models), there was more room for error, which may have limited the impact of the misclassification of the inversion strength. However, in Valley MTS, the underestimation of the inverted SLR likely contributed to higher probability of permafrost at treeline and at some higher elevations than in the local model.

The regional model did not perform well in Valley DN and Valley M222 likely because these valleys did not conform to assumptions made in the model. First, Valley DN was predicted to be above treeline in the regional model, and therefore was assumed to have a normal SLR. This led to low permafrost probability predictions in the valley bottom compared to AMGT in the local model. As a result, the valley was classified as discontinuous rather than continuous as in the local model. This misclassification is more likely a product of assuming a normal SLR rather than a discrepancy in the magnitude of the inverted SLR used. However, as Valley DN was still close to a sampling area for the regional model, it still largely captured the probability of permafrost overall better than in Valley M222. In Valley M222, the regional model predicted a high probability of permafrost throughout the valley except in a few areas at mid elevations, likely because it was misclassified as below treeline. Additionally, proximity of the closest sampled region for the regional model likely led to larger inaccuracies in this area. Some of the discrepancies between the two models in this valley may also be attributed to the more marginal permafrost in this valley as a small error in AMGT predictions may have led to the misclassification of permafrost absence. This may have resulted in the local model falling into sporadic permafrost, while the regional model classifies it as extensive discontinuous. The regional model, when compared to the local AMGT model, overestimated the probability of permafrost at high elevations potentially due to the weakly inverted SLR resulting in limited warming with elevation. Additionally, the high amount of snowfall and the shrub dominated landscape may have resulted in overall warmer ground conditions than would be predicted in the regional model if this valley was assumed to be partially below treeline (i.e., forested in the valley bottom). Overall, the regional model performed best in valleys where the elevation assumption of treeline, and therefore the spatial pattern of air and permafrost probability, held true. This was especially true at sites in relatively close proximity to a sampled region. The model performed the worst in valley bottoms classified as above treeline due to the assumption of a normal SLR in these valleys.

5.4. Comparison of AMGT spatial distribution pattern

The spatial distribution of AMGT for all four valleys were similar to a generally normal distribution (Fig. 10). The distribution for Valley DS was the most skewed with a long tail of cold temperatures generally present at high elevations, constituting a small portion of the landscape. Valley DN, Valley M222, and Valley MTS had a narrow range of temperatures with a normal distribution. The four valleys had a much different AMGT distribution than a similar size area at Cape Bounty, Melville Island, Nunavut (Garibaldi et al. 2021). The temperature distributions in Valley DN, Valley M222, and Valley MTS appear similar to that at Cape Bounty under climate

Fig. 10. Histograms for annual mean ground temperature (AMGT) in all four valleys and a High Arctic Site (Cape Bounty, NU) taken from Garibaldi et al. (2021).

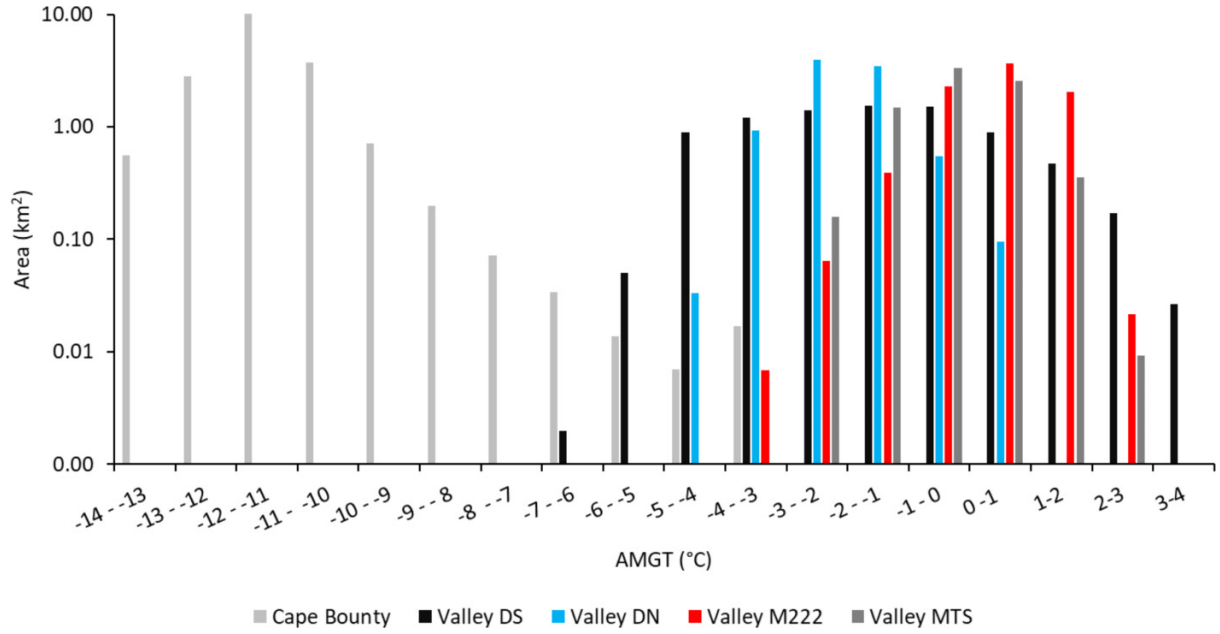

warming scenarios where the long tail of warm temperatures is reduced as larger portions of the landscape begin to warm. As such, the distribution curve shape in these valleys likely results from limited cold AMGT due to warmer air temperatures at exposed locations, while warm locations are protected or moderated from AMAT through high thermal and surface offsets. As a result, the distribution of ground temperatures is limited on both ends producing a normal distribution.

6. Conclusion

In mountain regions with annually inverted SLRs, the spatial distribution of the air and ground thermal regime is different from mountains under normal SLR conditions. As a result, an assumption of normality in high-latitude continental mountains such as those in Yukon results in an overprediction of permafrost presence based on measured air temperatures in the valley bottom and a misrepresentation of the spatial distribution of permafrost. However, the spatial distribution of the ground thermal regime is also dependent on snow cover, vegetation, and substrate properties, which may limit the impact of the inverted SLRs in certain valleys and locations. A regional model of permafrost probability agreed with the local AMGT models in valleys, meeting the assumptions made in the model creation, namely the position of treeline as an indicator of annually inverted SLRs. When the regional model correctly classified the SLR as inverted permafrost, probability more closely matched the local AMGT model even if the strength of the inverted SLR was largely underestimated. This is because permafrost was assumed to be present at the valley bottom and high elevations while absent at mid elevations at treeline. However, for valleys that did not conform to the regional model assumptions, discrepancies in the percentage and distribution of permafrost were large. Overall, this analysis highlighted that regional models can be an adequate predictor of local conditions, assuming the local areas conform to assumptions made in the regional model's creation. The spatial patterns of AMGT in these four valleys, as well as the assessment of the variable impact of the inverted SLR in each valley, may help guide other assessments of current ground temperature distributions and provide a more accurate starting point for studies of future warming in mountain valleys.

Acknowledgements

We acknowledge this research was conducted on the Tr'ondëk Hwëch'in, Acho Dene, and Dehcho First Nation settlement regions and traditional territories. We would like to thank the many field assistants who added in the data collection for this research, including A. Musk, S. Vegter, and O. Kienzle. Additionally, we would like to acknowledge the funding received through the Natural Science and Engineering Research Council of Canada (NSERC) as well as through the Northern Scientific Training Program (NSTP) through Polar Knowledge Canada and the University of Lethbridge.

Article information

History dates

Received: 1 November 2023
Accepted: 23 April 2024
Accepted manuscript online: 24 May 2024
Version of record online: 13 September 2024

Copyright

Data availability

The in situ GTN and air sensor data collected in all valleys in this study are available upon request from the corresponding author (madeleine.garibaldi@uleth.ca).

Author information

Author ORCIDs

Madeleine C. Garibaldi https://orcid.org/0000-0001-6801-2743
Philip P. Bonnaventure https://orcid.org/0000-0002-4157-0689
Nick C. Noad https://orcid.org/0000-0003-0652-5337

Author contributions

Conceptualization: MCG, PPB
Data curation: MCG, NCN
Formal analysis: MCG, PPB
Funding acquisition: PPB
Investigation: MCG, PPB, NCN
Methodology: MCG, PPB
Resources: WK
Software: WK
Supervision: PPB
Validation: MCG
Visualization: MCG
Writing – original draft: MCG
Writing – review & editing: MCG, PPB, NCN, WK

Competing interests

The authors declare there are no competing interests.

Supplementary material

Supplementary data are available with the article at https://doi.org/10.1139/as-2023-0067.

References

Apaloo, J., Brenning, A., and Bodin, X. 2012. Interactions between seasonal snow cover, ground surface temperature and topography (Andes of Santiago, Chile, 33.5° S). Permafrost and Periglacial Processes, **23**(4): 277–291. doi:10.1002/ppp.1753.

Barry, R.G. 2008. Mountain weather and climate. Cambridge University Press.

Bevington, A., and Lewkowicz, A.G. 2015. Assessment of a land cover driven TTOP model for mountain and lowland permafrost using field data, southern Yukon and northern British Columbia, Canada. *In* Paper presented at the Proceedings of GéoQuebec: 68th Canadian Geotechnical Conference and 7th Canadian Permafrost Conference. Quebec City, Canada.

Bonnaventure, P.P., and Lewkowicz, A.G. 2008. Mountain permafrost probability mapping using the BTS method in two climatically dissimilar locations, northwest Canada. Canadian Journal of Earth Sciences, **45**(4): 443–455. doi:10.1139/E08-013.

Bonnaventure, P.P., and Lewkowicz, A.G. 2011. Modelling climate change effects on the spatial distribution of mountain permafrost at three sites in northwest Canada. Climatic Change, **105**(1): 293–312. doi:10.1007/s10584-010-9818-5.

Bonnaventure, P.P., Lewkowicz, A.G., Kremer, M., and Sawada, M.C. 2012. A permafrost probability model for the southern Yukon and northern British Columbia, Canada. Permafrost and Periglacial Processes, **23**(1): 52–68. doi:10.1002/ppp.1733.

Bostock, H.S. 1966. Notes on glaciation in central Yukon Territory. **Vol. 65**, Department of Mines and Technical Surveys 1966, Ottawa.

Brown, J., Ferrians, O., Heginbottom, J., and Melnikov, E. 2002. Circum-Arctic map of permafrost and ground-ice conditions, version 2. National Snow and Ice Data Center, Boulder, Colorado, USA.

Burn, C.R., Moore, J.L., O'Neill, H.B., Hayley, D.W., Trimble, J.R., Calmels, F., Orban, S.N., and Idrees, M. 2015. Permafrost characterization of the Dempster Highway, Yukon and Northwest Territories. Paper presented at the 7th Canadian Permafrost Conference.

French, H.M. 2008. The periglacial environment. 3rd ed. John Wiley & Sons, Chichester, England.

Freudiger, D., Kohn, I., Seibert, J., Stahl, K., and Weiler, M. 2017. Snow redistribution for the hydrological modeling of alpine catchments. WIREs Water, **4**(5): e1232. doi:10.1002/wat2.1232.

Gądek, B., and Kędzia, S. 2008. Winter ground surface temperature regimes in the zone of sporadic discontinuous permafrost, Tatra Mountains (Poland and Slovakia). Permafrost and Periglacial Processes, **19**(3): 315–321. doi:10.1002/ppp.623.

Garibaldi, M.C., Bonnaventure, P.P., and Lamoureux, S.F. 2021. Utilizing the TTOP model to understand spatial permafrost temperature variability in a High Arctic landscape, Cape Bounty, Nunavut, Canada. Permafrost and Periglacial Processes, **32**(1): 19–34. doi:10.1002/ppp.2086.

Garibaldi, M.C., Bonnaventure, P.P., Smith, S.L., and Duchesne, C. 2022. Active layer variability and change in the Mackenzie Valley, Northwest Territories between 1991–2014: an ecoregional assessment. Arctic, Antarctic, and Alpine Research, **54**(1): 274–293. doi:10.1080/15230430.2022.2097156.

Government of Canada. 2015. Canadian Land Cover Circa 2000 (Vector)—Geobase Series, 1996–2005 [Dataset]. Natural Resources Canada. Available from https://open.canada.ca/data/en/dataset/97126362-5a85-4fe0-9dc2-915464cfdbb7 [accessed May 2019].

Government of Canada. 2016. Provinces/Territories, Cartographic Boundary File—2016 Census [Dataset]. Statistics Canada. Available from https://open.canada.ca/data/en/dataset/a883eb14-0c0e-45c4-b8c4-b54c4a819edb [accessed September 2019].

Government of Canada. 2017. Lakes, Rivers, and Glaciers in Canada—CanVec Series—Hydrographic Features [Dataset]. Natural Resources Canada. Available from https://open.canada.ca/data/en/dataset/9d96e8c9-22fe-4ad2-b5e8-94a6991b744b [accessed April 2019].

Government of Canada. 2017. Transport Networks in Canada—CanVec Series—Transport Features [Dataset]. Transport Canada. Available from https://open.canada.ca/data/en/dataset/c5c249c4-dea6-40a6-8fae-188a42030908 [accessed January 2019].

Government of Yukon. 2021. Yukon Communities [Dataset]. Geomatics Yukon. Available from https://open.yukon.ca/data/datasets/yukon-communities [accessed June 2022].

Gruber, S., and Haeberli, W. 2009. Mountain permafrost. Permafrost soils, 33–44. doi:10.1007/978-3-540-69371-0_3.

Heginbottom, J. 1995. Canada, permafrost: Canada Map Office.

Jenness, J. 2006. Topographic Position Index (tpi_jen.avx) extension for ArcView 3.x., v1.3a. Jenness Enterprises. Available from http://www.jennessent.com/arcview/tpi.htm.

Karunaratne, K., and Burn, C. 2003. Freezing *n*-factors in discontinuous permafrost terrain, Takhini River, Yukon Territory, Canada. *In* Paper presented at the Proceedings of the 8th International Conference on Permafrost.

Karunaratne, K.C., and Burn, C.R. 2004. Relations between air and surface temperature in discontinuous permafrost terrain near Mayo, Yukon Territory. Canadian Journal of Earth Sciences, **41**(12): 1437–1451. doi:10.1139/e04-082.

Lacelle, D., Lapalme, C., Davila, A.F., Pollard, W., Marinova, M., Heldmann, J., and McKay, C.P. 2016. Solar radiation and air and ground temperature relations in the cold and hyper-arid Quartermain Mountains, McMurdo Dry Valleys of Antarctica. Permafrost and Periglacial Processes, **27**(2): 163–176. doi:10.1002/ppp.1859.

Lewkowicz, A.G., and Ednie, M. 2004. Probability mapping of mountain permafrost using the BTS method, Wolf Creek, Yukon Territory,

Canada. Permafrost and Periglacial Processes, **15**(1): 67–80. doi:10.1002/ppp.480.

Lewkowicz, A.G., Bonnaventure, P.P., Smith, S.L., and Kuntz, Z. 2012. Spatial and thermal characteristics of mountain permafrost, northwest Canada. Geografiska Annaler: Series A, Physical Geography, **94**(2): 195–213. doi:10.1111/j.1468-0459.2012.00462.x.

Luetschg, M., Lehning, M., and Haeberli, W. 2008. A sensitivity study of factors influencing warm/thin permafrost in the Swiss Alps. Journal of Glaciology, **54**(187): 696–704. doi:10.3189/002214308786570881.

Mamet, S.D., Chun, K.P., Kershaw, G.G.L., Loranty, M.M., and Peter Kershaw, G. 2017. Recent Increases in Permafrost Thaw Rates and Areal Loss of Palsas in the Western Northwest Territories, Canada. Permafrost and Periglacial Processes, **28**(4): 619–633. doi:10.1002/ppp.1951.

Noad, N.C., and Bonnaventure, P.P. 2022. Surface temperature inversion characteristics in dissimilar valleys, Yukon Canada. Arctic Science, **8**(4): 1320–1339.

Noh, M.-J., and Howat, I.M. 2017. The surface extraction from TIN based search-space minimization (SETSM) algorithm. ISPRS Journal of Photogrammetry and Remote Sensing, **129**; 55–76. doi:10.1016/j.isprsjprs.2017.04.019.

O'Neill, H.B., Wolfe, S.A., and Duchesne, C. 2019a. New ground ice maps for Canada using a paleogeographic modelling approach. The Cryosphere, **13**(3): 753–773. doi:10.5194/tc-13-753-2019.

Obu, J., Westermann, S., Bartsch, A., Berdnikov, N., Christiansen, H.H., Dashtseren, A., et al.. 2019. Northern hemisphere permafrost map based on TTOP modelling for 2000–2016 at 1 km^2 scale. Earth-Science Reviews, **193**; 299–316. doi:10.1016/j.earscirev.2019.04.023.

Seppälä, M. 1982. An experimental study of the formation of palsas. *In* Paper presented at the Proceedings of the Fourth Canadian Permafrost Conference. National Research Council of Canada, Ottawa, Canada

Shur, Y.L., and Jorgenson, M.T. 2007. Patterns of permafrost formation and degradation in relation to climate and ecosystems. Permafrost and Periglacial Processes, **18**(1): 7–19. doi:10.1002/ppp.582.

Smith, M.W., and Riseborough, D.W. 2002. Climate and the limits of permafrost: a zonal analysis. Permafrost and Periglacial Processes, **13**(1): 1–15. doi:10.1002/ppp.410.

Vegter, S., Bonnaventure, P.P., Daly, S., and Kochtitzky, W. 2024. Modelling permafrost distribution using the temperature at top of permafrost model in the boreal forest environment of Whatì, NT. Arctic Science. doi:10.1139/as-2023-0010.

Wahl, H.E. 1987. Climate of Yukon. Environment Canada, Atmospheric Environment Service, 1987. 323pp.

Wang, T., Hamann, A., Spittlehouse, D., and Carroll, C. 2016. Locally downscaled and spatially customizable climate data for historical and future periods for North America. PLoS ONE, **11**(6): e0156720. doi:10.1371/journal.pone.0156720. PMID: 27275583.

Way, R.G., and Lewkowicz, AG. 2018. Environmental controls on ground temperature and permafrost in Labrador, northeast Canada. Permafrost and Periglacial Processes, **29**: 73–85. doi:10.1002/ppp.1972.

Yukon Ecoregions Working Group. 2004. Yukon Coastal Plain. *In* Ecoregions of the Yukon Territory: biophysical properties of Yukon landscapes. *Edited by* C.A.S. Smith, J.C. Meikle and C.F. Roots, Agriculture and Agri-Food Canada, PARC Technical Bulletin No. 04-01, Summerland, British Columbia, pp. 63–72.

Zhang, T. 2005. Influence of the seasonal snow cover on the ground thermal regime: an overview. Reviews of Geophysics, **43**(4): n/a–n/a. doi:10.1029/2004RG000157.